

Improving the dehydrogenation function and stability of Zn-modified ZSM-5 catalyst in methanol-to-aromatics reaction by Ca addition

Vicente, Héctor; Liu, Chuncheng; Gayubo, Ana G.; Castaño, Pedro; Pidko, Evgeny A.

DOI

[10.1016/j.apcata.2024.119854](https://doi.org/10.1016/j.apcata.2024.119854)

Publication date

2024

Document Version

Final published version

Published in

Applied Catalysis A: General

Citation (APA)

Vicente, H., Liu, C., Gayubo, A. G., Castaño, P., & Pidko, E. A. (2024). Improving the dehydrogenation function and stability of Zn-modified ZSM-5 catalyst in methanol-to-aromatics reaction by Ca addition. *Applied Catalysis A: General*, 683, Article 119854. <https://doi.org/10.1016/j.apcata.2024.119854>

Important note

To cite this publication, please use the final published version (if applicable). Please check the document version above.

Copyright

Other than for strictly personal use, it is not permitted to download, forward or distribute the text or part of it, without the consent of the author(s) and/or copyright holder(s), unless the work is under an open content license such as Creative Commons.

Takedown policy

Please contact us and provide details if you believe this document breaches copyrights. We will remove access to the work immediately and investigate your claim.



Improving the dehydrogenation function and stability of Zn-modified ZSM-5 catalyst in methanol-to-aromatics reaction by Ca addition

Héctor Vicente^{a,1,*}, Chuncheng Liu^{b,1}, Ana G. Gayubo^a, Pedro Castaño^{a,c}, Evgeny A. Pidko^{b,*}

^a Department of Chemical Engineering, University of the Basque Country (UPV/EHU), PO Box 644, Bilbao 48080, Spain

^b Inorganic Systems Engineering, Department of Chemical Engineering, Delft University of Technology, Delft 2629 Hz, the Netherlands

^c Multiscale Reaction Engineering, KAUST Catalysis Center, King Abdullah University of Science and Technology (KAUST), Thuwal 23955-6900, Saudi Arabia

ARTICLE INFO

Keywords:

Methanol-to-aromatics
Ethane dehydrogenation
ZSM-5
Catalyst deactivation
Dual-cycle mechanism

ABSTRACT

Adding Zn to the ZSM-5 zeolite effectively increases the aromatic selectivity in the methanol-to-aromatics (MTA) process. The formation of metal-derived Lewis acid sites promotes the dehydrogenation but at the cost of a rapid deactivation of the catalyst by coke, due to the increased aromatic formation. In this work, we impregnated a Zn-modified catalyst (2 wt%) with variable contents of Ca (0.02 and 0.5 wt%) and evaluated their kinetic behavior in the MTA and ethane dehydrogenation reactions. The results proved the superior performance of the Zn(2)Ca (0.02) catalyst due to a synergistic effect between the two metals. The Ca ions limit coke formation from excessive aromatization, increasing catalyst stability and removing Zn clusters, resulting in a recovery of Brønsted acid sites (BAS) active for the formation of light aromatics. Combining these effects results in a more efficient and viable catalyst for aromatic production from methanol.

1. Introduction

Light aromatics are essential building blocks for the petrochemical industry and contribute to the production of everyday goods such as medicines, surfactants, glues or polymers and are also an important part of the gasoline blend [1]. The most interesting aromatics are benzene, toluene, ethylbenzene and xylenes (BTEX), which high demand has led to the increasing use of naphtha reforming and steam cracking processes. These are non-sustainable technologies grounded in the use of fossil resources, mainly oil, which contribute to the emission of greenhouse effect gases and are dependent on changes in the geopolitical scenario. Therefore, developing alternative and competitive routes to produce these high-value aromatics is very interesting. The catalytic transformation of methanol into aromatics, or MTA reaction, is a promising technology for this transition, considering that methanol can be obtained by hydrogenating ambient CO₂ and biogas- or natural gas-derived syngas [2,3]. Methanol production and its subsequent upgrading into aromatics can become an environmentally friendly process decoupled from the oil-based industry, provided hydrogen production is sustainable.

The transformation of methanol into hydrocarbons is governed by a

series of fast auto-catalytic reactions involving the interaction between the methanol feed and the carbonaceous species confined in the zeolite pores [4,5], which are usually referred to in the literature as the hydrocarbon pool [6]. The reactions occurring in the hydrocarbon pool are controlled by the dual-cycle mechanism, which comprises two interconnected cycles: the olefin [7,8] and the aromatic cycles [9,10]. The olefin cycle depicts the methylation reactions of light olefins into more developed aliphatics and the possible cracking-oligomerization reactions between them. The aromatic cycle involves the methylation of aromatic species into alkylated aromatics, which can undergo dealkylation and ring contraction reactions to form light olefins. Both cycles are connected via the hydrogen transfer reaction, which consists of the formation of the first aromatics from a redistribution of hydrogen between the species formed in the olefin cycle [11,12]. The hydrogen transfer reaction yields hydrogen-rich paraffins, formed from the hydrogenation of light olefins, and hydrogen-poor cyclic species, formed from dehydrogenation and cyclization of aliphatics, that methylate into the first aromatic species, initiating the aromatic cycle.

Achieving a high aromatic yield is the main bottleneck of the process, as they are both main products and coke precursors. In addition, they are formed in parallel with the less valuable paraffins through hydrogen

* Corresponding authors.

E-mail addresses: hector.vicente@ehu.eus (H. Vicente), chunchengliu0524@outlook.com (C. Liu), anaguadalupe.gayubo@ehu.eus (A.G. Gayubo), pedro.castano@kaust.edu.sa (P. Castaño), E.A.Pidko@tudelft.nl (E.A. Pidko).

¹ These authors contributed equally to this work

<https://doi.org/10.1016/j.apcata.2024.119854>

Received 20 April 2024; Received in revised form 10 June 2024; Accepted 21 June 2024

Available online 22 June 2024

0926-860X/© 2024 The Author(s). Published by Elsevier B.V. This is an open access article under the CC BY license (<http://creativecommons.org/licenses/by/4.0/>).

transfer. During MTA, the catalyst is rapidly deactivated by coke formation, which occurs due to the successive methylation and polyaromatization of the aromatic species of the hydrocarbon pool [13]. Therefore, catalyst design plays an essential role in the MTA reaction, aiming on the one hand, to increase aromatic selectivity while inhibiting that of the paraffins, and on the other hand, to extend catalytic lifetime by limiting coke formation from aromatics.

The acidic ZSM-5 zeolite is one of the most frequently used catalysts for MTA, as its medium pore size helps the diffusion of aromatics and its interconnected cage-less channels limit the growth of poly-aromatic species [14]. Another great advantage of the ZSM-5 zeolite is that its physicochemical properties can be easily tuned, which makes it ideal for catalyst design. The acid strength and distribution can be modified by changing the Si/Al ratio of the zeolite [15,16], which also affects the density of Brønsted acid sites (BAS) and Lewis acid sites (LAS). It has been proved that a minimum of strong BAS is required for the correct development of the dual-cycle mechanism [17], as they promote the methylation and oligomerization reactions of light olefins towards aliphatics [18,19] and the activation of the aromatic cycle through the hydrogen transfer reaction of these aliphatics [19–21]. Introducing metal (M) ions into the ZSM-5 zeolite can alter the acidic properties. Several authors have reported a change in the MTA reaction mechanism towards a more selective formation of aromatics on Ga- [22–24], Ag- [25,26] or Zn- [27–29] modified catalysts. Among these, Zn-modified catalysts can be considered the most attractive option, given the relatively low price of zinc and its high abundance. The addition of Zn has been reported to increase the aromatic selectivity to over 60 %, depending on the preparation method and precursor salt used [30–34], compared to the usual 30–40 % obtained with the unmodified ZSM-5 zeolites under the same reaction conditions [35–37].

Despite the ongoing debate on the exact role of Zn in modifying the catalyst acidity [38,39], the consensus is that new LAS are formed, specifically Zn-LAS, from the exchange with the BAS in the parent zeolite. This Zn-LAS activates a dehydrogenation pathway, which converts the aliphatic intermediates into aromatics [33,40], and is favored over the hydrogen transfer route. Therefore, the undesired hydrogenation of olefin intermediates into paraffins in the MTA process is prevented.

Nevertheless, the enhanced aromatic formation speeds up the deactivation of the catalyst due to the high presence of aromatics in the reaction medium that contributes to coke formation. Several approaches have been reported to reduce the coke formation rate [41–43]. Still, most of them result in an excessive reduction of the acidic strength of the catalyst and, thus, a limitation of the aromatization reactions. A methodology currently under study uses dual-metal promoters, which use synergistic effects between metals to prolong the catalyst lifetime while maintaining high aromatic selectivity. The work of Xin et al. [44] detailed the synthesis and use of Zn-Sn/HZSM-5 catalysts with different Zn and Sn contents, achieving extended catalytic lifetimes (150 % increase) and maintaining high aromatic selectivity. These authors also reported the high regenerating capacity of their catalysts. Fan et al. [45] studied n-hexane conversion into aromatics using bimetallic [Zn, Cr]/H-ZSM-5 catalysts. They studied the effect of the Zn:Cr weight ratio for balancing the acid site distribution, obtaining improved BTEX selectivity values on their bimetallic catalysts during n-hexane conversion compared to the parent or the monometallic counterparts. In addition, they also observed increased conversion and lifetime when co-feeding MeOH with n-hexane. Liu et al. reported double the lifetime when adding Ca over Ga-modified catalysts in the MTA reaction while maintaining a high BTEX selectivity [46]. Their experimental results, supported by DFT calculations, attributed this effect to the formation of dual-metal cationic multinuclear species with moderate dehydrogenation activity. In addition, the incorporation of Ca over ZSM-5 zeolite has been reported to restrain the reactions of the aromatic cycle [47,48], inhibiting the coke formation rate of the catalyst. Although this applies to most of alkaline earth metals [21,47], it has been reported in the

literature that the Ca atoms trigger an effect referred to as “pore occupation” [49]. This effect causes the adsorption of water, methanol, and methoxy group molecules by Ca atoms, which increase in size and are retained in the structure of the zeolite, thus limiting the excessive methylation of light aromatics into bulkier ones.

In this work, we have studied the catalytic activity and stability of a dual-metal-promoted ZSM-5 catalyst for the MTA process. We considered Zn the most attractive and cost-efficient primary metal for dehydrogenation promotion. We investigated the co-promotion of a Zn-modified ZSM-5 catalyst with Ca, which was selected as the promising secondary metal for limiting aromatization. The physicochemical properties of the synthesized catalysts with varying Ca and Zn contents were characterized with a particular focus on the effect of the incorporation of metals on catalyst acidity and BAS and LAS distribution. The catalytic properties of the mono- and dual-metal-modified zeolite catalysts and their impact on the results of the catalytic tests were investigated in detail and compared with those of the parent H-form of the zeolite. The obtained results formed a basis for discussing the mechanistic impact of the combined incorporation of Zn and Ca and the potential synergy between metals for the MTA process.

2. Experimental

2.1. Catalyst preparation

The ammonium form of the ZSM-5 zeolite (NH₄-ZSM-5) with a Si/Al ratio of 15 (Zeolyst International, CBV 3024E) was used to prepare the protonic form (H-ZSM-5, denoted as ‘Parent’) as well as the metal-modified (Zn/ZSM-5, Ca/ZSM-5 and Ca-Zn/ZSM-5) catalysts. The protonic form of ZSM-5 zeolite was prepared by calcination at 575 °C for 2 h (ramp of 5 °C min⁻¹) in order to make them thermally stable.

The Zn-modified ZSM-5 was prepared by performing two consecutive ion exchanges over the NH₄-ZSM-5 in an aqueous solution with excess of Zn(NO₃)₂·6 H₂O (Sigma-Aldrich, ACS reagent, 99 %, 36 g in 1 L of de-ionized H₂O) at 80 °C for 1 h [35]. According to the authors, the catalyst obtained after the two consecutive ion exchanges shows the highest aromatic selectivity, given by its optimal BAS/LAS ratio. After each ion exchange step, the sample was filtered and washed in de-ionized H₂O at 80 °C for 1 h and dried at 110 °C overnight. After the second ion exchange, the sample was calcined for 2 h at 450 °C, with a heating ramp of 5 °C min⁻¹.

Ca-containing samples were prepared by the incipient wetness impregnation method with Ca(NO₃)₂·4 H₂O (Sigma-Aldrich, ACS reagent, 99 %) solution and dried at 80 °C overnight [46]. The impregnation of Ca was performed on the parent zeolite and the Zn-modified zeolite catalyst, using different Ca contents. Before to the characterization and catalytic testing, the modified samples were also calcined following the previous procedure mentioned for the parent H-ZSM-5. These samples were denoted as Zn(2) for the Zn ion-exchanged zeolite catalyst, Ca(0.5) for the Ca impregnated zeolite catalyst, and Zn(2)Ca(0.02) and Zn(2)Ca(0.5) for the zeolite catalysts modified with both Zn and Ca, with the number in parentheses representing the nominal wt% of each metal in each of the samples.

Additionally, we synthesized a Zn-modified H-ZSM-5 zeolite using the impregnation method, to compare the impact of the state of Zn species in the catalyst in the performance of the MTA reaction. We followed the methodology described by Valecillos et al. [34], aimed at obtaining a 2 wt% of Zn in the resulting catalyst, which was denoted as Zn(2)_(Impregnation).

2.2. Catalyst characterization

The crystalline properties of the catalysts were analyzed by X-ray diffraction (XRD) using a Bruker D8 Advance diffractometer equipped with a Germanium primary monochromator, Bragg-Brentano geometry and a X-ray tube with a Cu anticathode.

The elemental compositions of as-prepared samples were determined by inductively coupled plasma atomic emission spectrometry (ICP-AES) using a Perkin Elmer Optima 5300DV instrument (glass torch + Sapphire injector). For the measurement, ca. 50 mg of the sample was digested in an aqueous solution of 4.5 mL 30 % HCl, 1.5 mL 65 % HNO₃ and 0.2 mL 40 % HF using a microwave heater operating at the maximum power for 1 h, and diluted afterward in 50 mL of de-ionized water.

The porous properties were analyzed by N₂ physisorption in a Tristar II 3020 at −196 °C. Before the analysis, the samples were dried and degassed at 350 °C for 6 h under a N₂ stream.

The catalyst acidity and acid site distribution were determined by NH₃ adsorption-desorption in a chemisorption analyzer (Micromeritics, Autochem II 2920), coupled with a ThermoStar GSD320 mass spectrometer (Pfeiffer Vacuum). The procedure involved introducing the sample in the glass reactor and heating it to 550 °C for 1 h with a ramp of 10 °C min^{−1} in a He atmosphere to strip the water adsorbed from the pores and remove any remaining impurities. Afterwards, the sample was cooled to 150 °C and NH₃ was injected with a flowrate of 0.05 cm³ min^{−1}. Once the sample was saturated, the injection of NH₃ was stopped and the sample was swept with He to desorb the physisorbed NH₃. Subsequently, the desorption stage was started, heating the sample to 550 °C with a heating ramp of 5 °C min^{−1} under a He stream. The acidic strength of the catalyst was deduced by deconvolution of the peaks appearing in the profile obtained by following the ammonia signal in the mass spectrometer (corresponding to *m/z* = 15). The peaks appearing at lower desorption temperatures correspond to acid sites of weak nature, whereas those at higher temperatures correspond to acid sites of strong nature.

The acid site nature of the samples was evaluated by FTIR spectroscopy of adsorbed pyridine (anhydrous, Sigma-Aldrich, 99.8 %) or Py-FTIR in a Nicolet 6700 FTIR (Thermo Scientific) equipped with an extended KBr beam splitting and an MCT detector. For the analysis, ca. 20 mg of the sample was pressed into a self-supporting wafer (1.6 cm diameter) and placed into an IR quartz cell. Before pyridine adsorption, the sample was activated at 400 °C (heating ramp of 1 °C min^{−1}) for 7 h under vacuum and then cooled to room temperature. A known volume of pyridine gas was then dosed into the sample-containing section. After stabilization of the pyridine, the sample was heated at 160 °C for 1 h, and the spectra were collected at room temperature. The amount of BAS and LAS was derived from the integrated absorbance of the peaks measured at 1545 and in the 1458–1446 cm^{−1} region, respectively, using the Emeis correlation [50] and the corresponding extinction coefficients (0.73 and 1.11 for BAS and LAS, respectively):

$$BAS = \frac{A_B \cdot S_{sample}}{\epsilon_B \cdot m_{sample}} \quad (1)$$

$$LAS = \frac{A_L \cdot S_{sample}}{\epsilon_L \cdot m_{sample}} \quad (2)$$

Where *S*_{sample} and *m*_{sample} are the surface and the weight of the analyzed sample, respectively. *A* is the integrated area of the peak and *ε* is the molar extinction coefficient, with the sub index B and L, referred to the BAS and LAS, respectively.

Additionally, we measured the properties of the Zn species by X-ray photoelectron spectroscopy (XPS) in a SPECS system (Berlin, Germany) equipped with a Phoibos 150 1D-DLD analyzer and a monochromatic radiation source of Al Kα (1486.7 eV) using a step energy of 0.1 eV, dwell time of 0.1 s and a pass energy of 30 eV.

2.3. Catalytic tests

The catalytic runs were performed using a fixed-bed reactor setup. A 4 mm (ID) quartz reactor tube was filled with the catalyst (particle size 150–212 μm), using 40 mg for the MTA tests and 100 mg for the ethane

dehydrogenation tests. For the MTA tests, reaction temperatures of 400 and 450 °C were used, with a methanol (MeOH, Sigma-Aldrich, ACS reagent, ≥ 99.8 %) inlet partial pressure of 5.2 kPa in He and a WHSV (weight hourly space velocity) value of 1 g_{MeOH} g^{−1} h^{−1}. For the ethane dehydrogenation reactions, an ethane flow with a partial pressure of 5 kPa in He was fed to the catalyst bed (WHSV = 0.5 g_{Eth} g^{−1} h^{−1}) at 440, 500 and 540 °C.

Before the reaction, the catalyst was activated in 50 mL min^{−1} of air at 550 °C (heating ramp of 5 °C min^{−1}) for 2 h to sweep any impurities or water from the catalyst.

For analyzing the results, the following reaction indices were defined:

The conversion of oxygenated species, accounting both MeOH and DME (dimethyl ether) in the MTA reactions, and conversion of ethane for the dehydrogenation reactions (*X*_{Ox} and *X*_{Ethane}, respectively):

$$X_{Ox} = \frac{F - F_{DME} - F_{MeOH}}{F} \cdot 100 \quad (3)$$

$$X_{Ethane} = \frac{F - F_{Ethane}}{F} \cdot 100 \quad (4)$$

carbon-based yield of each product *i* (*Y*_{*i*}):

$$Y_i = \frac{F_i}{F} \cdot 100 \quad (5)$$

and carbon-based selectivity of each product *i* (*S*_{*i*}):

$$S_i = \frac{Y_i}{X} \cdot 100 = \frac{F_i}{F - F_{DME} - F_{MeOH}} \cdot 100 \quad (6)$$

where *F* represents the total carbon-based molar flowrate at the inlet, *F*_{*i*} denotes the carbon-based molar flowrate of each species *i* or lump and *F*_{DME}, *F*_{MeOH} and *F*_{Ethane} are the carbon-based molar flowrates of DME, MeOH and ethane, respectively, at the reactor outlet.

Moreover, the hydrogen transfer index (HTI) was used to measure the shift in the impact of the hydrogen transfer and dehydrogenation reactions, which is defined as the paraffin to olefin ratio:

$$HTI_k = \frac{F_{C_k^-}}{F_{C_k^=}} \quad (7)$$

where, *F*_{C_k[−]} and *F*_{C_k⁼} are the total carbon-based molar flowrate of paraffins and olefins, respectively, referred to the *k* number of C atoms.

3. Results

3.1. Catalyst characterization

XRD characterization of the catalyst samples (Figure S1 in the Supplementary Material) indicates the preservation of the MFI structure after the modification with cations [49]. The XRD patterns reveal some small decrease in the peak intensities after the incorporation of metals, which is coherent with the previous results in the literature [51,52]. No marked bands corresponding to ZnO are detected through XRD, which typically appear in the 30–40° range, according to Yuan and Lobo [53].

The metal content measured by ICP and the surface properties measured by N₂ physisorption for the synthesized catalysts are summarized in Table 1, with the corresponding N₂ adsorption-desorption isotherms presented in Figure S2. The ICP analysis shows the expected loadings of Zn and Ca in the zeolite materials. The surface properties of the metal-modified catalyst did not exhibit significant differences from the parent H-ZSM-5, neither after the ion exchange nor after the impregnation procedures. All samples presented a high specific surface (*S*_{BET} around 400 m² g^{−1}), with a predominance of micropores over mesopores (micropore surface, *S*_{microp}, and volume, *V*_{microp}, between 313 and 340 m² g^{−1} and 0.13–0.14 cm³ g^{−1}, respectively).

The results for the characterization of the acidic properties using

Table 1

Metal content and surface properties of the parent H-ZSM-5 zeolite (Si/Al = 15) and the mono- and dual-metal-modified ZSM-5 catalysts with different Zn and Ca contents.

	Zn (wt)	Ca (wt)	S_{BET} (m^2 g^{-1})	S_{Ext} (m^2 g^{-1})	V_{total} (cm^3 g^{-1})	V_{microp} (cm^3 g^{-1})
Parent	-	0	388	74.9	0.17	0.14
Ca(0.5)	-	0.5	356	75	0.16	0.13
Zn(2)Ca(0.5)	1.8	0.49	365	64	0.16	0.13
Zn(2)Ca (0.02)	2.0	0.01	370	63.4	0.16	0.14
Zn(2)	2.0	0	366	68.4	0.16	0.14

NH_3 -TPD and Py-FTIR are presented in Fig. 1, with the corresponding values of the total acidity and acid site distribution in Table 2. For the results of the Py-FTIR (Fig. 1a), the parent H-ZSM-5 presents a wide band at 1545 cm^{-1} , corresponding to the BAS ($660 \mu\text{mol g}^{-1}$), with a small band at 1455 cm^{-1} , corresponding to the pyridine adsorbed on LAS (ca. $20 \mu\text{mol g}^{-1}$) due to the extra-framework Al [54]. When 0.5 wt % Ca is incorporated, the band at 1545 cm^{-1} is reduced and a new band at 1447 cm^{-1} appears [55], evidencing the exchange of BAS with the Ca-LAS [48], resulting in a BAS/LAS ratio close to unity (around $370 \mu\text{mol g}^{-1}$ for each type of acid site). For the Zn(2) zeolite catalyst, the almost complete elimination of the pyridine band corresponding to the BAS at 1545 cm^{-1} is observed in the FTIR spectrum, with an enhancement of the band at 1455 cm^{-1} due to the formation of Zn-LAS [35,39],

Table 2

Total acidity and acid site density distribution (in $\mu\text{mol g}^{-1}$) of the parent H-ZSM-5 zeolite (Si/Al = 15) and the mono- and dual-metal-modified ZSM-5 catalysts with different Zn and Ca contents.

	NH_3 -TPD			FTIR			
	Total	WAS	MAS	SAS	Total	LAS	BAS
Parent	686	260	68	358	685	21	664
Ca(0.5)	783	229	240	314	699	331	368
Zn(2)Ca(0.5)	870	286	455	129	1231	1024	207
Zn(2)Ca(0.02)	787	446	211	130	974	768	206
Zn(2)	714	319	307	89	733	617	116

which evidences the high exchange of Zn cations. The analysis of the Py-FTIR data for the catalysts with 1, 2 and 3 % of Zn (Figure S3) reveals that the maximum degree of Zn exchange is achieved for 2 wt%, in line with the literature [35]. This indicates that Zn contents lower than 2 wt % would not achieve the maximum formation of Zn-LAS essential for enhancing the dehydrogenation pathway and thus increasing the aromatic formation. On the contrary, Zn contents over 2 wt% would promote the formation of Zn clusters that would hinder the activity of the catalyst, which was also concluded in the results of Pinilla-Herrero et al. [35]. The quantification of the spectral data reveals the BAS density reduction in Zn(2) zeolite catalyst to $100 \mu\text{mol g}^{-1}$ with a concomitant increase of LAS density to $620 \mu\text{mol g}^{-1}$. The high-intensity band due to Zn-LAS is also detected for the dual-metal Zn(2)Ca(0.02) catalyst, which does not show separate bands attributable to Ca-LAS. The Zn-LAS and Ca-LAS species were simultaneously observed only at higher Ca loading

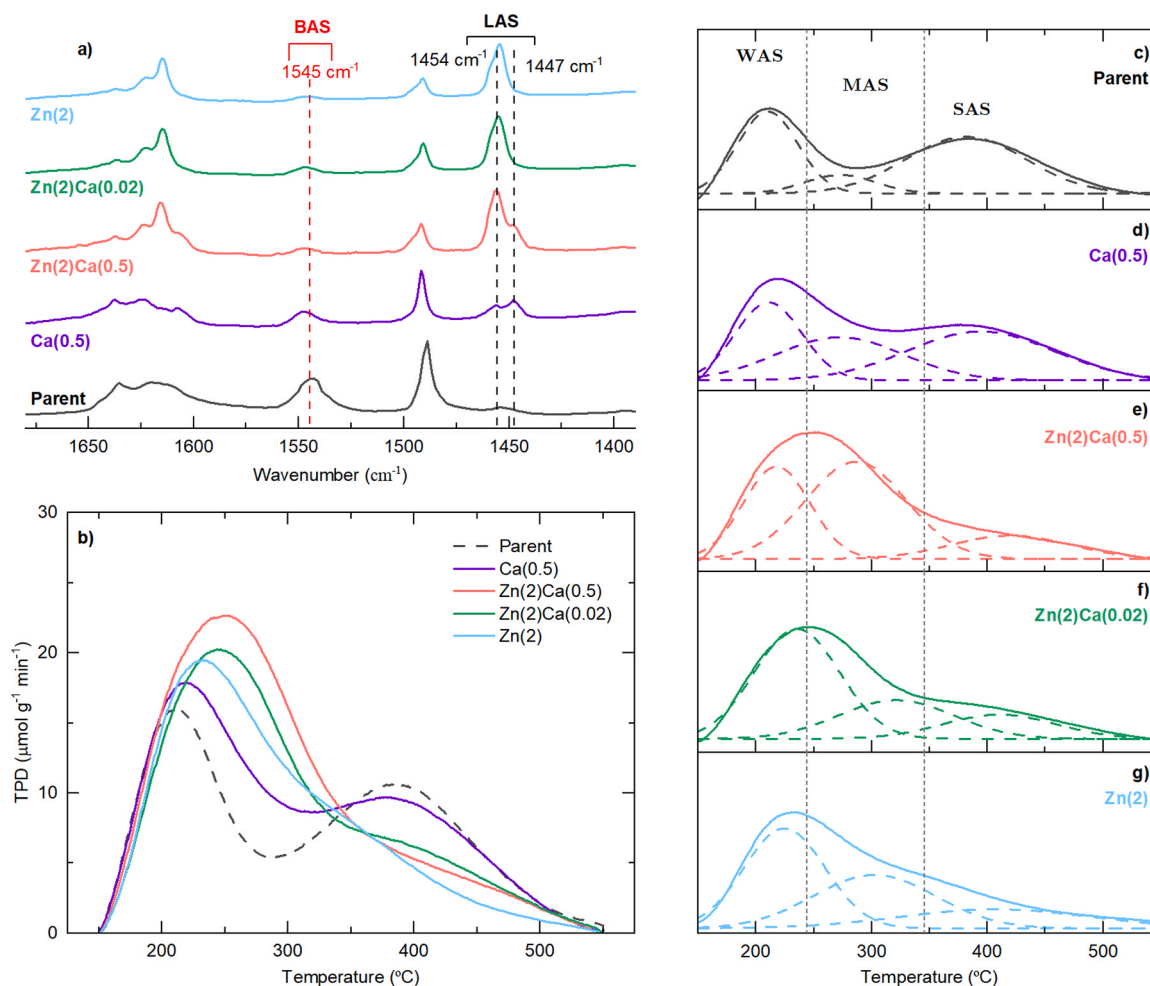


Fig. 1. (a) Py-FTIR spectra at $160 \text{ }^{\circ}\text{C}$, (b) NH_3 -TPD profiles and (c-g) deconvoluted NH_3 -TPD profiles for the parent H-ZSM-5 zeolite (Si/Al = 15) and the mono- and dual-metal-modified ZSM-5 catalysts with different Zn and Ca contents.

in the Zn(2)Ca(0.5) catalyst. Interestingly, both LAS and BAS densities are higher for the dual-metal Zn(2)Ca(0.02) and Zn(2)Ca(0.5) catalysts compared to Zn(2).

The acidity characterization with NH₃-TPD (Fig. 1b) reveals two distinguishable peaks in the TPD profiles of the parent H-ZSM-5 (dashed black line), which correspond to acid sites of different strengths. When metal atoms, either Zn or Ca, are incorporated into the zeolite, an increase of the peak at low temperature is observed, alongside a decrease of the peak at high temperature. By deconvoluting the NH₃-TPD signals in Fig. 1b for each catalyst (Fig. 1c-g), we identified three different peaks corresponding to acid sites of different strengths: weak acid sites (WAS) with the maximum below 250 °C, medium acid sites (MAS) with the maximum in the 250–360 °C range and strong acid sites (SAS) with the maximum above 360 °C. The parent H-ZSM-5 has mostly WAS and SAS, with few MAS (see values in Table 2). The specific impact of Ca addition is observed in the Ca(0.5) catalyst, for which the band in the MAS region increases (acid site density of 240 μmol g⁻¹), whereas those of the WAS and SAS decrease (229 and 314 μmol g⁻¹, respectively). When Zn is incorporated in the Zn(2) catalyst, the density of SAS is significantly decreased (89 μmol g⁻¹), and those of the WAS and MAS increase (319 and 307 μmol g⁻¹, respectively). The bi-metallic catalysts have the highest total density of acid sites, with a predominance of WAS and MAS over SAS, but with a different distribution of WAS and MAS between them. The Zn(2)Ca(0.5) has the highest density of MAS (455 μmol g⁻¹) and of LAS (1024 μmol g⁻¹), indicating the formation of LAS of medium acidity at high Zn and Ca contents. On the contrary, the Zn(2)Ca(0.02) catalyst shows the highest density of WAS (446 μmol g⁻¹), even higher than the Zn(2) catalyst, but a more moderate density of MAS (211 μmol g⁻¹).

Overall, the incorporation of metals causes an exchange of BAS into new LAS of weak and medium acidity [34,36,37]. A Ca content of up to 0.5 wt% causes mostly the formation of LAS of medium acidity with a moderate reduction of BAS. On the contrary, incorporating Zn up to 2 wt

% results in an exchange of BAS, mainly strong ones, for weak and medium acidity LAS. The effect of the impregnation with Ca of the Zn-modified catalyst differs depending on the amount of Ca added. In the case of the Zn(2)Ca(0.5) catalyst, the results correspond to the combined effect of adding both metals, with this catalyst exhibiting a high density of WAS and MAS being formed from both Zn and Ca. For the Zn(2)Ca(0.02) catalyst, the density of MAS decreases compared to the Zn(2) catalyst, but that for the WAS increases up to 446 μmol g⁻¹ (the highest value). Interestingly, for both bi-metallic catalysts, there is an increase in SAS and BAS densities compared to the monometallic Zn-modified catalyst. This could indicate that the introduction of Ca partially recovered some of the strong BAS that may have been neutralized during the ion exchange with Zn⁺² due to the formation of Zn clusters. This is also observed in IR spectra in the 3400–3800 cm⁻¹ region of the IR spectra (Figure S4), which shows the OH-group bands. When comparing the Zn(2) catalyst with the parent zeolite in this region, we observed the decrease in intensity of the band at 3611 cm⁻¹, which is attributed to the Si-O(H)-Al groups related to BAS [56]. This result is in agreement with the decrease in BAS density observed in Fig. 1 and Table 2. Moreover, the intensity of this band again increases when Ca is added, also corresponding with the partial recovery of BAS observed in our results in the 1370–1680 cm⁻¹ region of the IR during pyridine adsorption (Fig. 1a). The partial recovery effect is similar to that reported for Ni and Fe modifications over P-ZSM-5 catalysts [57,58]. The Zn clusters could be acting as acid sites of medium acidity, explaining the slight decrease of MAS observed for the Zn(2)Ca(0.02) catalyst compared to the Zn(2) upon Ca addition. Moreover, it could also explain the increase of WAS and LAS densities observed for the Zn(2)Ca(0.02) catalyst compared to the Zn(2) catalyst, which could indicate that the removal of Zn clusters is also facilitating the access of the molecules to part of the Zn-LAS.

The results of the Zn 2p_{3/2} spectra obtained by XPS analyses, shown in Fig. 2, provide further information on the Zn species formed.

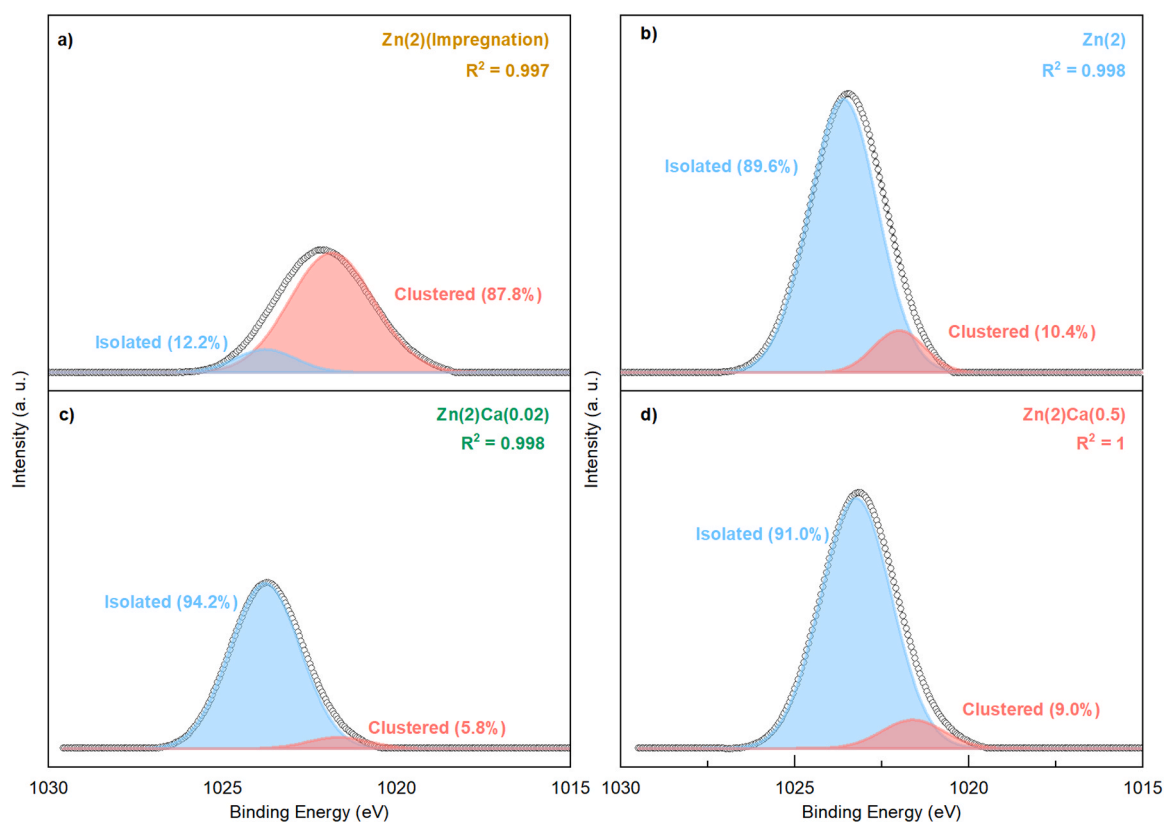


Fig. 2. Zn 2p_{3/2} spectra for the (a, b) mono- and (c, d) dual-metal-modified ZSM-5 catalysts with different Ca contents.

According to the literature [59,60], the band in the 1020–1025 eV range can be deconvoluted into two separate peaks. The peak with a maximum at 1023 eV can be attributed to well-dispersed isolated Zn ions, mostly responsible for the dehydrogenation function. The peak at 1021 eV is assigned to clustered Zn species with lower dehydrogenation activity. The data in Fig. 2a reveals that the catalyst prepared by impregnation has mainly clustered Zn species, whereas the ones prepared by ion exchange have mostly isolated Zn ions. Additional information regarding the comparison of the acidic properties obtained with the Zn(2)_(Impregnation) and the Zn(2) and parent catalysts is presented in Figure S5. The NH₃-TPD and Py-FTIR results (Figure S5a and S5b, respectively) show that both Zn addition methods reduce the amount of strong BAS. Nevertheless, only the Zn(2) catalyst presents the corresponding increase of weak LAS sites, corresponding to the well-dispersed Zn atoms that activate the dehydrogenation pathway [33,40]. Interestingly, the impregnation with Ca increases the percentage of isolated Zn ions compared to the mono-metallic Zn(2) catalyst and is maximum for the Zn(2)Ca(0.02) catalyst (Fig. 2c). This agrees with the increased density of weak LAS previously observed in Table 2 for this catalyst. These sites are Zn-LAS sites, which are the main sites that cause the promotion of the dehydrogenation reactions [37,61].

3.2. Catalytic testing

We next investigated the catalytic behavior of the parent H-ZSM-5 and the metal-modified catalysts in the MTA reaction at 400 and 450 °C, with the results of the catalytic tests presented in Figs. 3 and 4.

Fig. 3a shows the evolution of the conversion of oxygenates with time-on-stream (TOS) at 450 °C, with the corresponding yield of each product lump at the beginning of the reaction (TOS = 10 min) in Fig. 3c. Metal modification has a pronounced effect on the stability of the catalyst, measured as the total time to trigger deactivation (decrease from complete conversion). The parent H-ZSM-5 maintains complete conversion for 40 h, whereas the conversion in the case of metal-modified catalysts drops to 20 % after less than 12 h. When comparing the mono- and bi-metallic catalysts, the order of stability is Zn(2)Ca(0.02) > Zn(2) > Zn(2)Ca(0.5), with the drop in conversion observed at 8.7, 5.1 and 3 h, respectively.

The results of the yields at the beginning of the reaction (TOS = 10 min) (Fig. 3c) help to explain the different times at complete conversion obtained with the studied catalysts. All the metal-modified catalysts show a lower yield of light paraffins (C₂⁻–C₄⁻ lump, including ethane, propane, and butanes) than the parent H-ZSM-5 and a higher yield of aromatics (A lump, including BTEX and trimethyl- and

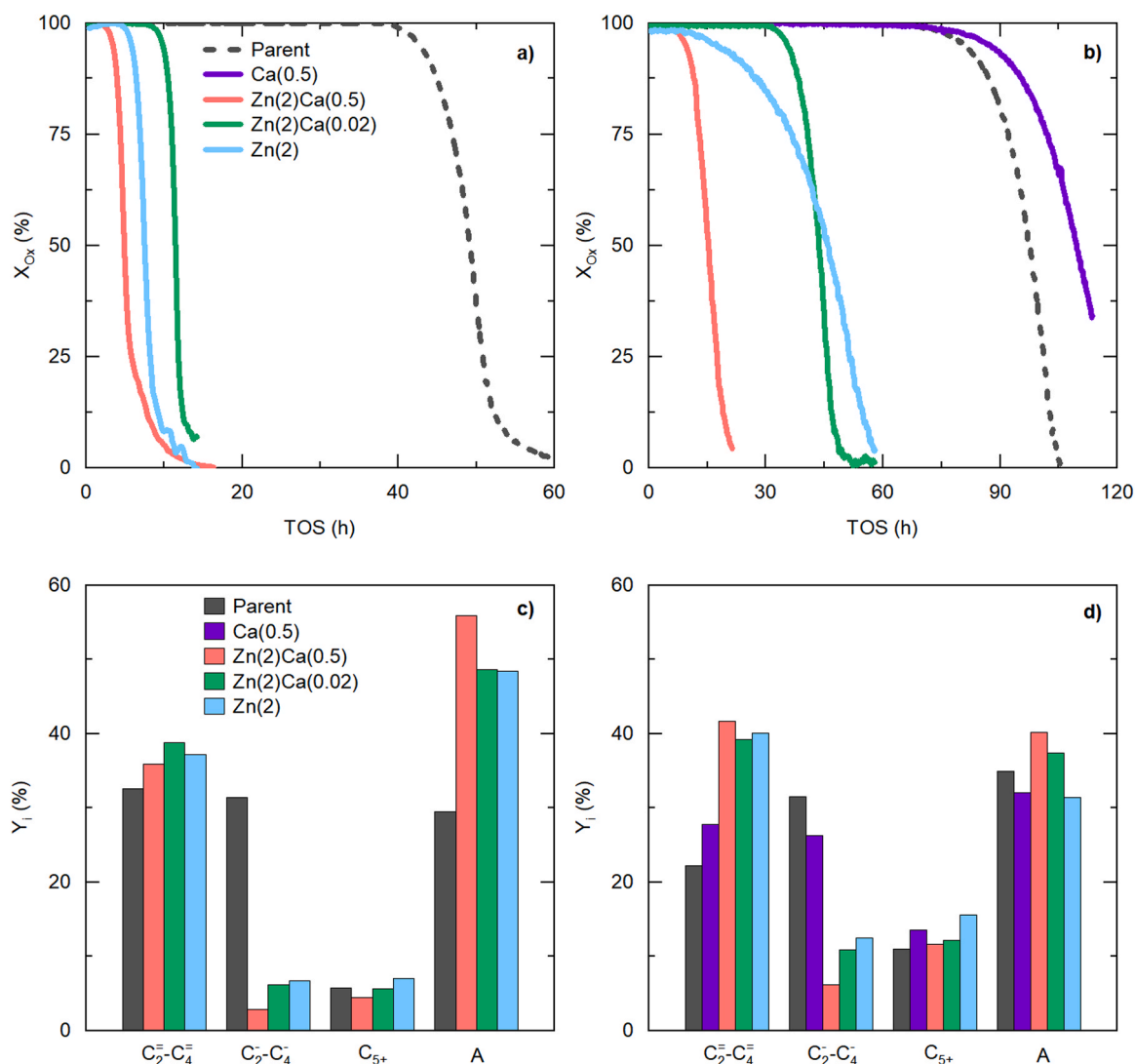


Fig. 3. (a, b) Evolution of the oxygenate conversion with TOS and (c, d) carbon-based yields of main products at the beginning of the reaction (TOS = 10 min) for the parent H-ZSM-5 zeolite (Si/Al = 15) and the mono- and dual-metal-modified ZSM-5 catalysts. Reaction conditions: P_{MeOH} = 5.2 kPa, m_{cat} = 40 mg, WHSV = 1 g_{MeOH} h⁻¹ g⁻¹, N₂ flowrate = 10 mL min⁻¹, (a, c) 450 °C and (b, d) 400 °C.

tetramethyl-benzenes) at the beginning of the reaction. This marked difference in the initial yields of these two lumps indicates the promotion of the dehydrogenation pathway upon adding Zn. This was not the case for the catalyst prepared by Zn impregnation (Figure S6), which still showed a high initial yield towards light paraffins, in a similar ratio with aromatics compared to the parent zeolite (Figure S6b). Interestingly, the Zn(2)_(Impregnation) catalyst shows a higher yield towards aromatics and paraffins than the parent zeolite, with a lower time until complete deactivation. The ZnO cluster species, which are predominant in the Zn(2)_(Impregnation) catalyst, could also act as adsorption sites for water molecules during the reaction [62]. The lower presence of water in the reaction medium could decrease the competitive adsorption with the active hydrocarbon pool species, increasing the rate of the hydrogen transfer reaction and thus, the paraffin and aromatic yields. In addition, it could also hinder the stability of the catalyst, as water adsorption over the ZnO clusters would decrease the effect of water in attenuating coke formation. Moreover, the yield of light olefins (C₂⁻–C₄⁻ lump, including ethylene, propylene and butenes) is also slightly higher on the Zn-modified catalysts, which correlates to the lower degree of hydrogenation of this lump into the C₂⁻–C₄⁻ lump. Interestingly, the yield of heavy aliphatic compounds (C₅⁺ lump, including every aliphatic with five or more carbon atoms) is similar for all catalysts. This is a positive outcome, as it may indicate that despite the shift in the predominant mechanism for aromatic formation (from the hydrogen transfer to the dehydrogenation pathway) the aliphatic intermediates are converted at a similar rate. Additional information on product distribution is presented in Table S1 in the Supplementary Information. Among the light olefins, propylene is the major compound, with similar yields of ethylene and butenes at 400 °C, but higher yield for ethylene than butenes at 450 °C. Regarding the light paraffins, the yields follow the order butanes > propane > ethane. In the A lump, the xylenes are the major component, followed by trimethyl- and tetramethyl-benzenes and toluene.

Based on these results, we considered that the differences in the catalyst stability are due to two leading causes. First, the higher concentration of aromatics on the metal-modified catalyst could contribute to coke formation by further methylation into polyaromatics [63,64]. The higher presence of coke was proven by analyzing the coke deposited in the sample after each reaction. Since the total TOS differed, we used the averaged coke deposition rate, defined as the ratio between the coke amount deposited and the reaction duration [65,66]. The results for these average coke deposition rates (Figure S7) evidence the higher coke deposition rate for the metal-modified catalysts compared to the parent one.

The change in the acid site distribution is the second possible cause of the difference in catalyst stability. The combined characterization of the catalyst acidity by NH₃-TPD and Py-FTIR, in Table 2, showed a significant decrease of strong BAS when the catalyst is modified with Zn (SAS drop from 358 to 89–130 μmol g⁻¹ and BAS from 660 to 100–200 μmol g⁻¹). These acid sites are the main sites responsible for the activity of the reactions in the hydrocarbon pool [17,19]. Thus, removing these sites could contribute to the more rapid loss of complete conversion conditions. This assumption also explains the differences observed between mono- and bi-metallic catalysts. For the Zn(2)Ca(0.02) catalyst, the higher strong BAS density observed compared to the Zn(2) catalyst, probably due to the partial recovery of active sites when a small amount of Ca is added, directly correlates with the almost twice higher stability obtained compared to that of the Zn(2) zeolite catalyst.

The increase of the Ca content in the Zn(2)Ca(0.5) catalyst does not further increase the stability, as no further recovery of BAS is observed at higher Ca contents. On the contrary, the Zn(2)Ca(0.5) catalyst shows the fastest loss of complete conversion and a high coke deposition rate (Figure S7), in agreement with this catalyst having the highest initial yield of aromatics (Fig. 3c). A possible explanation for this behavior could be that the Ca-LAS of medium acidic strength formed when adding high Ca loadings (Figs. 1a and 1e) act as adsorption sites for water. The

preferential adsorption of water over these sites rather than on the strong BAS of the zeolite could limit water's attenuating effect on coke deposition [67,68], accelerating the coke formation rate and causing a faster catalyst deactivation. The pore occupation effect, addressed by Liutkova et al. [49], is caused by the preferential adsorption of water, oxygenates, and methoxy species over the Ca atoms. These authors observed this pore occupation effect at Ca loadings over 0.5 wt%, so this effect would not be significant with the Zn(2)Ca(0.02) zeolite catalyst, and thus, a higher lifetime is achieved with this catalyst.

The Ca(0.5) catalyst was not used for the catalytic testing at 450 °C as its lack of dehydrogenating capacity observed at 400 °C (Figs. 3b and 3d) would not promote the aromatics selectivity. In Fig. 3d, it can be observed that the Ca(0.5) catalyst still yields a high amount of light paraffins (26 %), which is close to that of the parent H-ZSM-5 (31 %). Moreover, the yield of aromatics obtained over Ca(0.5) is also lower than that of the parent H-ZSM-5, whereas the yields of light olefins and C₅⁺ aliphatics are lower over the latter. These results indicate that the Ca addition slows down the reactions of the hydrocarbon pool towards the final products of the reaction, in this case the aromatics and light paraffins formed by the hydrogen transfer mechanism. This trend was also observed by Yarulina et al. [48], who used Ca addition to enhance the MTO (methanol-to-olefins) process by limiting aromatization reactions, and by Liutkova et al. [69], who proved the lower activity of the hydrogen-transfer reactions at 450 °C over Ca-modified ZSM-5 catalysts with Si/Al = 25. These authors also observed increased lifetimes on their Ca-doped catalysts, caused by the decreased aromatic formation, which is also observed in our results over Ca(0.5) (see Fig. 3d) compared to the parent zeolite. The stability trend observed for the low-temperature MeOH conversion by Zn-modified catalysts is similar to that for the reactions at 450 °C. In this case, since the Zn incorporation triggers the dehydrogenation pathway, the aromatic formation is promoted, resulting in accelerated catalyst deactivation and the sudden drop of the oxygenate conversion. The performance is again improved by minor doping with Ca. Indeed, Zn(2)Ca(0.02) zeolite catalyst performs better than either Zn(2) or Zn(2)Ca(0.5) catalysts, with the latter showing the highest deactivation rate. In general, the onset of deactivation is shifted to longer TOS for MeOH conversion at a lower temperature of 400 °C (compare Figs. 3a and 3b), indicating the attenuated formation of poly-aromatics, which act as the main coke precursors, slowing down the deactivation rate [70]. Interestingly, the change in catalytic lifetime upon Ca addition is opposite on the Ca(0.5) catalyst and the Zn(2)Ca(0.5) catalyst. When considering the Ca(0.5) catalyst, the addition of Ca over the parent H-ZSM-5 zeolite causes the exchange of Brønsted acid sites present in the zeolite for Ca-LAS and a slight decrease in strong acids sites (see Fig. 1 and Table 2), which are the main active sites for the formation of aromatics through the hydrogen-transfer mechanism. At the same time, the pore occupation effect caused by Ca limits the formation of bulky polyaromatics. Thus, the two combined effects reduce the formation of polyaromatics that could convert into coke precursor species, improving catalyst lifetime. On the contrary, for the Zn(2)Ca(0.5) catalyst, the addition of Ca over a Zn-modified catalyst, Zn(2) catalyst in this case, does not cause any exchange of acid sites with Ca, as the exchange already happened upon Zn addition, leading to the formation of Zn- Lewis acid sites that promote aromatic formation through the dehydrogenation pathway. Therefore, in the Zn(2)Ca(0.5) catalyst, the pore occupation effect occurs on a catalyst where aromatic formation is promoted instead of restrained. This is detrimental to the process, as the combination of both increased aromatization and pore occupation effect rapidly saturates the zeolite pores and limits the access of the reactants to the active sites, causing a fast deactivation of the catalyst.

To further compare the differences caused by the metal modification of the catalyst, we analyzed the evolution of the carbon-based selectivity values of the main products with the conversion at 450 °C (Fig. 4). For comparison, the results for the evolution of product selectivity with TOS is presented in Figures S8 and S9, for the reactions carried out at 400 and 450 °C, respectively. The evolution of the light olefin selectivity (in

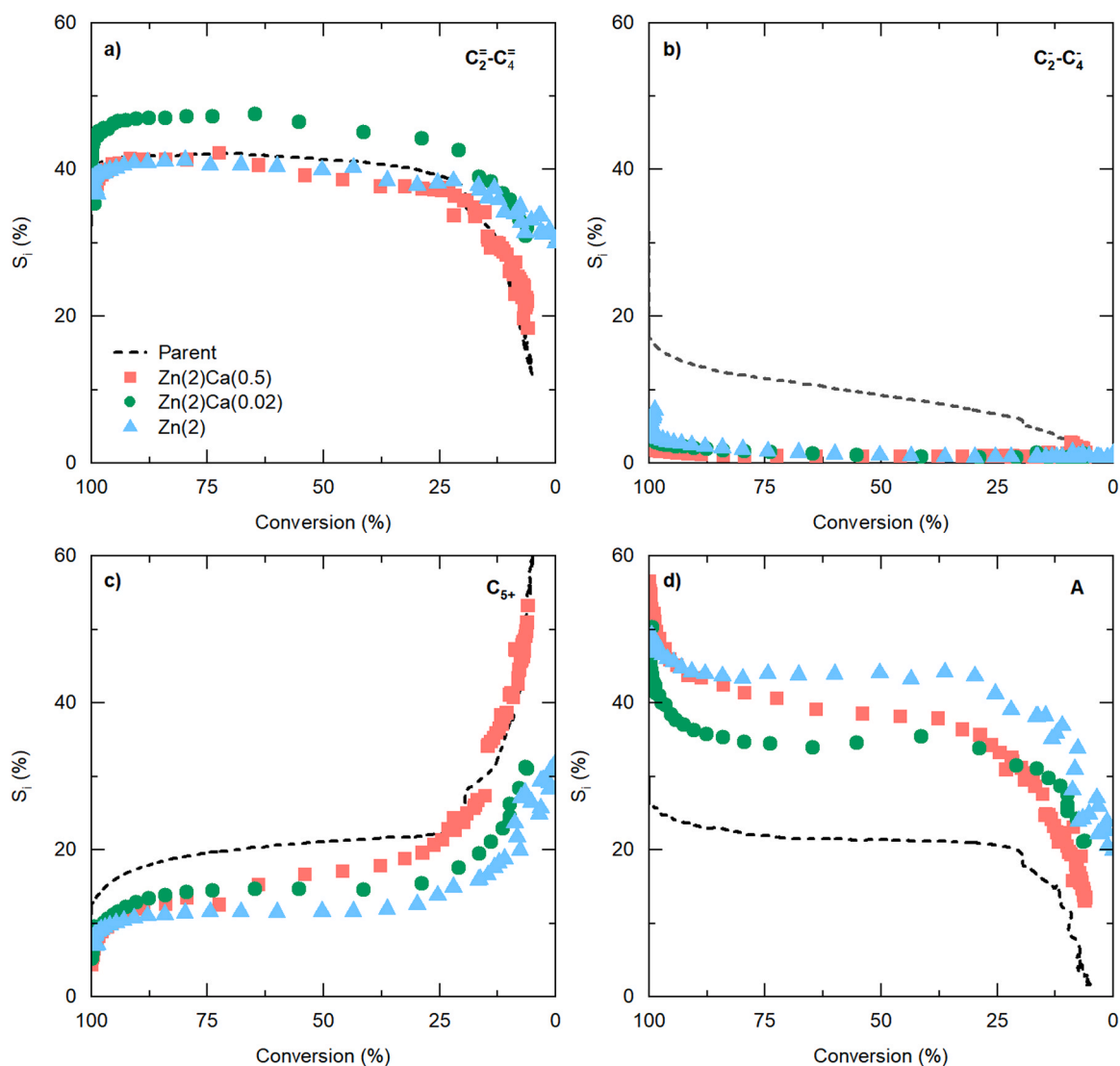


Fig. 4. Evolution with oxygenate conversion of the carbon-based selectivity to (a) light olefins (C_2-C_4), (b) light paraffins (C_2-C_4), (c) C_{5+} aliphatics and (d) aromatics (A) in MeOH conversion by parent H-ZSM-5 zeolite (Si/Al = 15) and the mono- and dual-metal-modified ZSM-5 catalysts. Reaction conditions: 450 °C, P_{MeOH} = 5.2 kPa, m_{cat} = 40 mg, $WHSV = 1 \text{ g}_{MeOH} \text{ h}^{-1} \text{ g}^{-1}$, N_2 flowrate = 10 mL min^{-1} .

Fig. 4a) shows little difference between the four catalysts, except for the Zn(2)Ca(0.02) catalyst, on which the selectivity values are higher after complete conversion is lost. In contrast, a notable drop in the selectivity of light paraffins is obtained (in Fig. 4b) for the Zn-modified catalysts compared to the parent H-ZSM-5. In contrast, the presence of Zn promotes aromatic selectivity (Fig. 4d), which reaches values of over 48 % at complete conversion compared to the ca. 30 % for the parent zeolite. This trend evidences the enhancement of the dehydrogenation route upon Zn addition, which is maintained at all conversion levels. This suggests that the dehydrogenating capacity is not lost before the catalyst completely deactivates by coke deposition. This is not the case when comparing the results obtained at 400 °C with the Ca(0.5) catalyst to the Zn(2) catalyst, for which relatively high paraffin selectivity values are obtained (Figure S8b). In addition, the light olefin selectivity values are low (Figure S8a), closer to those of the parent catalyst. The evolution of the selectivity of C_{5+} aliphatics (Fig. 4c) has an opposite trend to that of aromatics. This can be attributed to the increased conversion of aliphatic intermediates caused by promoting the dehydrogenation route in the Zn-containing catalysts.

Comparing the results obtained for the mono- and dual-metal catalysts, the Zn(2)Ca(0.02) and Zn(2)Ca(0.5) catalysts show a higher initial

aromatic selectivity than the Zn(2) catalyst (see Figure 4d and Figure S9d). These two catalysts presented the highest density BAS (Table 2), which were recovered after Ca addition. The strong BAS are the main sites responsible for the activity of the reactions in the hydrocarbon pool [18,19,21], which explains the highest aromatic selectivity obtained with the bi-metallic catalysts compared to the parent and the Zn(2) catalysts. Nevertheless, after complete conversion is lost, the dual-metal catalysts show lower selectivity to aromatics at mid-low conversion levels than the Zn(2) catalyst, which indicates that, even at low Ca loadings, the aromatization reactions are restrained [48,49]. In addition, the higher C_{5+} aliphatic selectivity observed for the Zn(2)Ca(0.5) catalyst compared to the Zn(2)Ca(0.02) catalyst at that conversion range (Fig. 4c) could point to a decrease in the cracking rate of heavier aliphatics [46]. This explains the low light olefin selectivity observed at higher Ca contents (Fig. 4a). Additionally, the higher aromatic selectivity achieved at complete conversion (Fig. 3c and Figure S9d) with the Zn(2)Ca(0.5) catalyst could be due to the aforementioned preferential adsorption of water over Ca-LAS instead of over the strong BAS of the zeolite [49], which would mitigate the attenuating effect of water for the formation of products [67,71]. The additional aromatics formed would contribute to the coke formation and deactivation of the catalyst [72,

73], thus explaining the faster decay of the aromatics selectivity at conversion levels below 25 % (Fig. 4d) and the fast deactivation observed in Fig. 3a and in Figure S9 when this catalyst is used. This causes selectivity to aromatics over Zn(2)Ca(0.5) catalyst to decrease below that obtained with the Zn(2) and Zn(2)Ca(0.02) catalysts after only 6 h (Figure S9d) and, similarly, that of light olefins (Figure S9a).

Despite the metal-modified catalysts having such a low stability, they are more efficient producing aromatics than the parent H-ZSM-5 zeolite. The results for the cumulative yield of the main lumps (evaluated by integrating the product yield curves with TOS before conversion drops below 20 %) corresponding to the reactions at 450 °C and 400 °C are presented in Figs. 5a and 5b, respectively, with the catalyst lifetime (measured as the TOS before MeOH conversion drops below 20 %) in the dashed arrows. It can be observed that the cumulative aromatics yield for the catalytic tests performed at 450 °C (Fig. 5a) are higher than those for the tests at 400 °C (Fig. 5b). At the latter temperature, the cumulative yield of olefins and C₅₊ aliphatics for the metal-modified catalysts is higher than for the parent zeolite. This might indicate that at such a low temperature, the extent of the reactions for the conversion of

intermediates is low due to the lower acidic strength of the metal modified catalysts, and thus higher temperatures could be required to promote the aromatization reactions further. As observed in Fig. 5b, at 400 °C, the cumulative yield for the paraffins is much lower on the Zn-containing samples than on the parent or the Ca(0.5) catalyst, which points to a change of mechanism caused by Zn, but not by Ca-modification. At 450 °C (Fig. 5a) the cumulative yield of aromatics for the metal-modified catalysts is almost twice that of the parent H-ZSM-5 zeolite, implying that the former can produce more aromatics per gram of catalyst used than the latter. The Zn(2)Ca(0.02) catalyst shows the highest cumulative aromatic yield, indicating that it is a more efficient catalyst for aromatic production. The increased BAS density when adding Ca makes it more stable than the Zn(2) catalyst, and minimizing the Ca loading avoids the detrimental effect caused by Ca interaction with the oxygenates and water. Moreover, the Zn(2)Ca(0.02) catalyst also presents a higher value for forming light olefins, potentially forming more aromatics at lower WHSV values.

The HTI is commonly used to compare the relevance of the hydrogen transfer reactions among catalysts [4,35]. In this case, we calculated the HTI for the species of two, three, and four C atoms and the sum of the three, with the selectivity values at the beginning of the reaction (TOS = 10 min) for each catalyst. The values of the HTI obtained for the parent H-ZSM-5 zeolite are higher than those obtained for the metal-modified catalysts (Fig. 6), thus proving the promotion of the dehydrogenation route over the hydrogen transfer reactions on the Zn-containing zeolites. Among the metal-modified zeolite catalysts, the mono-metallic Zn(2) has, overall, a higher value of HTI than the bi-metallic zeolite catalysts (note the lower scale for the C₂ and C₃ species). The lower HTI values obtained when Ca is added are coherent with an overall decrease of the acid strength, which restrains the hydrogen transfer reactions of the aliphatics [48,49], thus lowering the formation of light paraffins. This also agrees with the higher selectivity of C₅₊ aliphatics observed in the bi-metallic catalysts (Fig. 4c and Figure S9) when conversion drops below 90 %, which is more marked on the Zn(2)Ca(0.5) zeolite catalyst, which presents the lowest HTI values.

To check the hypothesis on the influence of Ca addition on the dehydrogenation activity of the Zn-modified catalysts, we analyzed their intrinsic kinetics towards such transformations using ethane dehydrogenation as a model reaction. The results of these reactions are summarized in Fig. 7 and correspond to the mean values obtained in

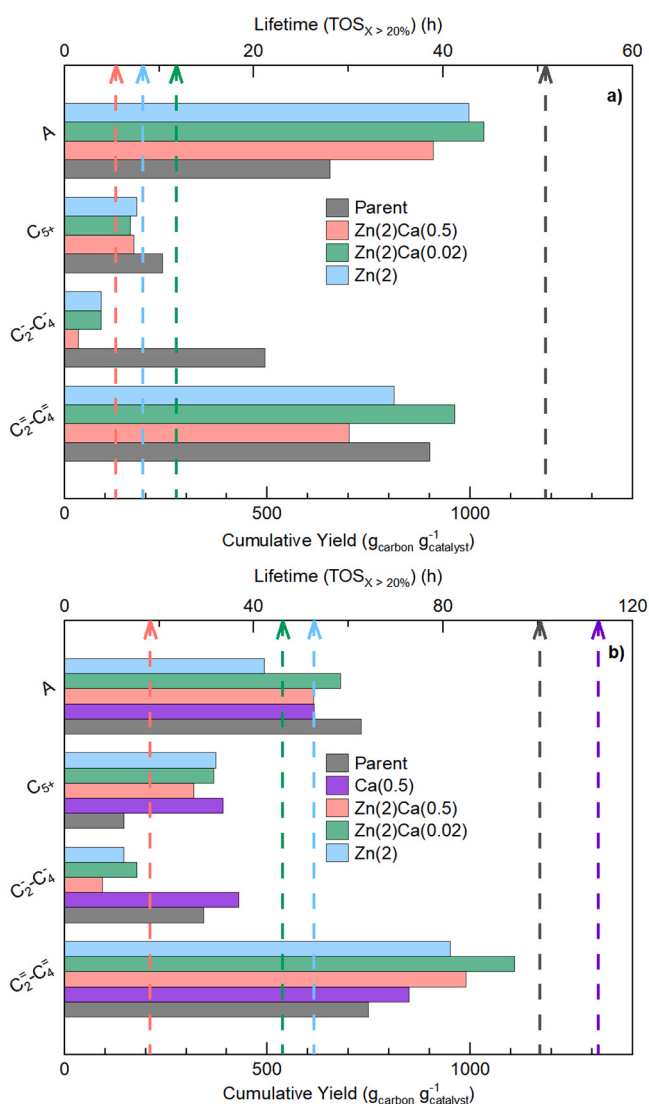


Fig. 5. Cumulative yields of the main product lumps (bars) and lifetime (dashed arrows), measured as the TOS before conversion drops below 20 %, during MeOH conversion at (a) 450 °C and (b) 400 °C by parent H-ZSM-5 zeolite (Si/Al = 15) and the mono- and dual-metal-modified ZSM-5 catalysts. Reaction conditions: P_{MeOH} = 5.2 kPa, m_{cat} = 40 mg, WHSV = 1 g_{MeOH} h⁻¹ g⁻¹, N₂ flowrate = 10 mL min⁻¹.

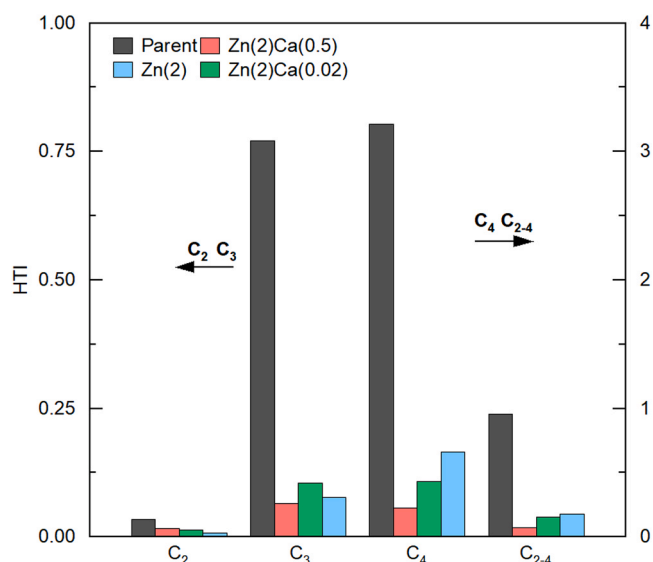


Fig. 6. Hydrogen transfer index (HTI) of C₂, C₃, and C₄ species for the parent H-ZSM-5 (Si/Al = 15) zeolite and the mono- and dual-metal-modified ZSM-5 catalysts. Reaction conditions: 450 °C, P_{MeOH} = 5.2 kPa, m_{cat} = 40 mg, WHSV = 1 g_{MeOH} h⁻¹ g⁻¹, N₂ flowrate = 10 mL min⁻¹.

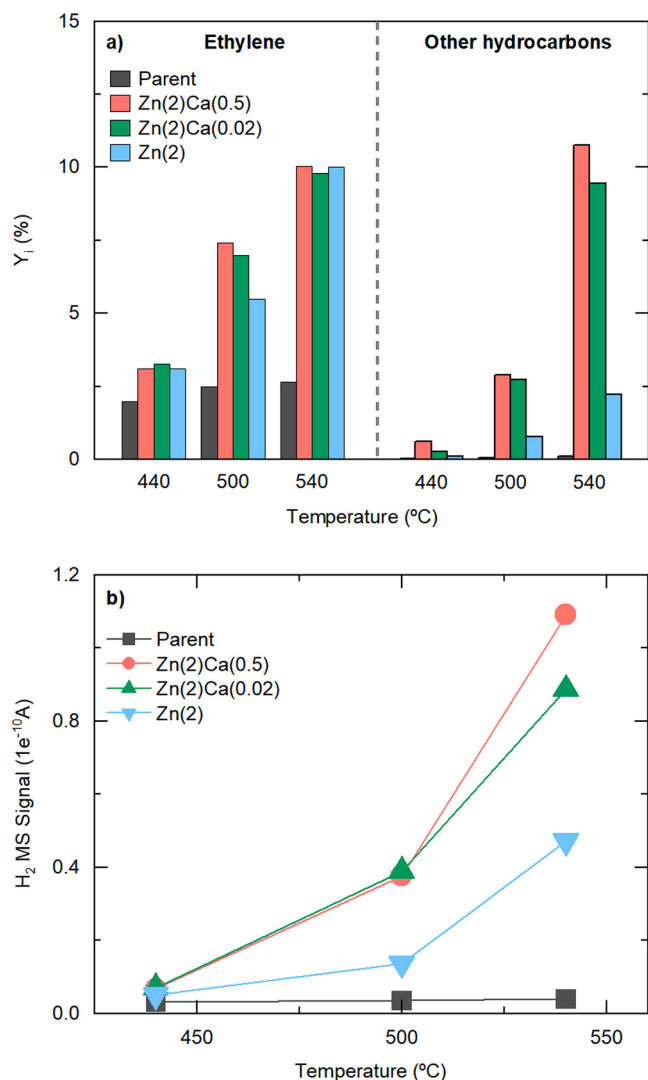


Fig. 7. (a) Mean carbon-based yields of ethylene and other hydrocarbon products and (b) H₂ output signal for the dehydrogenation of ethane at different temperatures over the parent H-ZSM-5 zeolite (Si/Al = 15) and the mono- and dual-metal-modified ZSM-5 catalysts. Reaction conditions: P_{ethane} = 5 kPa, m_{cat} = 100 mg, WHSV = 0.5 g_{Ethane} h⁻¹ g_{cat}⁻¹.

successive steps with increasing temperature. Sufficiently high WHSV values were used to avoid catalyst deactivation in each step for all the catalysts (as shown in the conversion profiles in Figure S10), allowing a more detailed study of the intrinsic kinetics and reactivity of the catalysts.

Fig. 7a summarizes the mean carbon-based yields of ethylene (left part of the graph) and other hydrocarbon products (right part of the graph), and Fig. 7b reports the signal of the hydrogen at the outlet of the reactor measured with a mass spectrometer coupled with the GC analyzer. The ethylene yield over metal-modified catalysts increases from ca. 3 % at 440 °C to 5–7.5 % and 10 % at 500 and 540 °C, respectively. While ethylene yields are comparable for the metal-modified catalysts, the Ca addition significantly impacts the formation of other hydrocarbon products, comprising ca. 65 % of benzene and toluene, 20 % of methane and 15 % of propane and propylene. This is attributed to the increased BAS with the addition of 0.02 wt% Ca, which promote the oligomerization and aromatization reactions of the ethylene that is formed by dehydrogenation of ethane in the exchanged Zn acid sites [18,20,21].

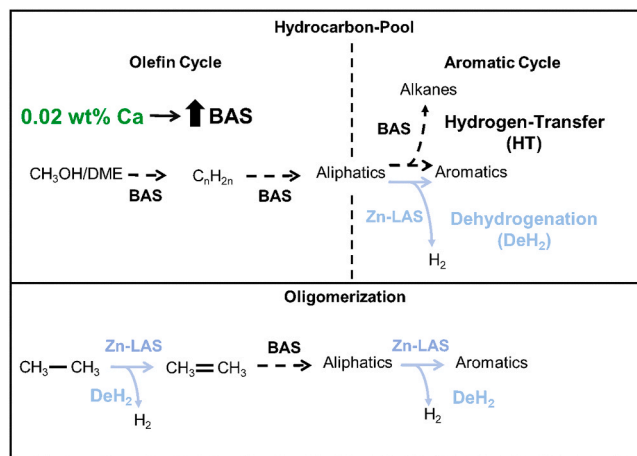
The dehydrogenation activity of BAS is negligible, as evidenced by the very low H₂ output observed with the parent H-ZSM-5 zeolite

(Fig. 7b). The low ethane conversion in this case is provided by the hydrogen transfer route [11], which agrees with the high values of HTI obtained for the parent zeolite (Fig. 6). The rapid increase in ethane conversion and simultaneous H₂ formation above 500 °C is evidence of promoting the dehydrogenation mechanism by Zn addition.

4. Discussion

Based on all these results, we propose a mechanism, depicted in Scheme 1, for the MTA and ethane dehydrogenation reactions on Ca-Zn/ZSM-5 zeolite catalysts. The introduction of Zn-LAS to the ZSM-5 zeolite promotes the dehydrogenation reactions in the MTA process, thus increasing the formation of aromatics and inhibiting the formation of light paraffins. This increased dehydrogenating capacity is evident from the strong enhancement of ethane conversion into ethylene for Zn-modified zeolites compared to the parent material. The decrease of BAS density, mainly strong sites, with the addition of Zn, reduces the overall activity of the catalyst for the dual cycle reactions [19,74], which explains the rapid decay of the complete conversion in the MTA reaction and the low formation of other hydrocarbons in the ethane dehydrogenation with the Zn(2) catalyst. With the Zn(2)Ca(0.02) catalyst, the low amount of Ca interacts with Zn, causing an increase in catalyst stability, similar to what was previously reported for Ca interaction with Ga [46]. Although the exact mechanism of this interaction is unclear, the higher stability of the Zn(2)Ca(0.02) catalyst compared to the Zn(2) catalyst can be attributed to the partial recovery of strong BAS upon the addition of Ca by a cleaning effect of Zn clusters formed during Zn addition [75]. This would increase the density of acid sites that promote the reactions of the dual cycle [15,16,19], thus prolonging the time at complete conversion in MTA and also promoting the secondary reactions upon ethane dehydrogenation to form heavier hydrocarbons (ca. 65 % benzene and toluene) [29,76].

Another factor that could extend the catalyst lifetime is the partial suppression of the excessive aromatization reactions caused by Ca addition [48]. The pore occupation effect caused by incorporating Ca atoms into the structure of the ZSM-5 attenuates the formation of larger aromatics that act as coke precursors and slows down the deactivation by coke formation [13,49]. Nevertheless, this effect is expected negligible when the Zn(2)Ca(0.02) catalyst is used due to the low Ca loading. On the contrary, with Zn(2)Ca(0.5) catalyst is used due to the low Ca loading. This preferential adsorption would counteract the effect of water in attenuating coke deposition via competitive adsorption on the strong BAS of



Scheme 1. Proposed reaction path for MTA and ethane dehydrogenation on Ca-Zn/ZSM-5 catalyst (Si/Al = 15). Black dashed arrows indicate the reactions on BAS and blue solid arrows indicate the reactions on LAS.

the zeolite [67,68].

The bulky Ca particles formed when adsorbing water would reduce the pore space in the reaction medium, leading to excessive aromatic condensation. This increases aromatic selectivity (as observed for the Zn (2)Ca(0.5) catalyst in Figs. 3c and 4d) and, subsequently, accelerates catalyst deactivation [72,73].

5. Conclusions

The metal modification by co-promotion of Ca over Zn/ZSM-5 catalysts provides an exciting method to improve the MTA reaction by increasing the selectivity towards aromatics of high economic value while maintaining control of the deactivation by coke deposition. The Zn cations promote the dehydrogenation route, thus avoiding the undesired parallel formation of light paraffins through the hydrogen transfer mechanism and, at the same time, the Ca balances the acid site distribution and the aromatization capacity of the catalyst, thus limiting the deactivation by coke formation. The promoting role of Zn on the dehydrogenation paths was supported by the increased H₂ output observed during ethane dehydrogenation with the Zn-containing catalysts, compared to the parent zeolite, and was higher in the dual-metal catalysts, especially at 540 °C.

Incorporation of only a 0.02 wt% of Ca alongside Zn helps to stabilize the catalyst, almost doubling the time at complete conversion in the MTA reaction compared to the mono-metallic catalyst, whereas further addition of Ca up to 0.5 wt% leads to an excessively rapid deactivation of the catalyst. The superior performance obtained by adding small amounts of Ca can be explained by the synergistic effect between Zn and Ca, which causes a partial recovery of the strong BAS lost after adding Zn. This increases the density of acid sites available for the reactions of the dual cycle mechanism to occur. Conversely, when the Ca loading is high, the Ca-LAS formed upon Ca addition potentially act as adsorption sites for the water on the reaction medium, which causes the formation of big Ca particles. As a result, catalyst stability is overall reduced, both by reducing the effect of water in attenuating coke formation and by the limited pore space in the zeolite, which increases the formation of condensed aromatic molecules.

We conclude that the addition of small amounts of Ca is an efficient method to extend the catalytic lifetime of Zn-modified catalysts for the MTA process, as it balances the density of strong BAS and weak Zn-LAS, thus creating a good compromise between the slight loss of aromatization capacity, caused by Ca, and the reduced coking of the catalyst. This leads to a catalyst with high productivity of aromatics obtained per unit of catalyst used, which is a determining factor that can significantly reduce the operating costs when considering the industrial implementation of the process.

Funding Sources

This work was supported by the Department of Education and Investigation of the Basque Government (Project IT1645-22 and PhD grant PRE_2021_2_0133 and EGONLABUR(2021-2022) for H. Vicente), and by King Abdullah University of Science and Technology (KAUST).

CRedit authorship contribution statement

Pedro Castaño: Writing – review & editing, Supervision, Resources. **Chuncheng Liu:** Writing – review & editing, Investigation, Formal analysis, Conceptualization. **Ana G. Gayubo:** Writing – review & editing, Supervision, Investigation. **Héctor Vicente:** Writing – review & editing, Writing – original draft, Investigation, Formal analysis. **Evgeny Alexandrovich Pidko:** Writing – review & editing, Supervision, Resources, Formal analysis, Conceptualization.

Declaration of Competing Interest

The authors declare that they have no known competing financial interests or personal relationships that could have appeared to influence the work reported in this paper.

Data availability

Data will be made available on request.

Acknowledgment

This work was carried out thanks to the financial support of the all the funding sources (Department of Education and Investigation of the Basque Government and King Abdullah University of Science and Technology (KAUST)). The authors also thank the technical and human support provided by SGIker (UPV/EHU-ERDF, EU).

Supplementary material

Additional results regarding the characterization of extra properties and catalytic testing of the parent H-form and mono- and dual-metal-modified catalysts under methanol and ethane transformation reactions, and the deactivation by coke formation after methanol-to-aromatics reactions with these catalysts.

Appendix A. Supporting information

Supplementary data associated with this article can be found in the online version at doi:10.1016/j.apcata.2024.119854.

References

- [1] T. Li, T. Shoinkhorova, J. Gascon, J. Ruiz-Martinez, *ACS Catal.* **11** (2021) 7780–7819.
- [2] A.M. Niziolek, O. Onel, Y.A. Guzman, C.A. Floudas, *Energ. Fuel.* **30** (2016) 4970–4998.
- [3] G. Leonzio, *J. CO₂ Util.* **27** (2018) 326–354.
- [4] S. Ilias, A. Bhan, *ACS Catal.* **3** (2013) 18–31.
- [5] M. Zhang, S. Xu, Y. Wei, J. Li, J. Wang, W. Zhang, S. Gao, Z. Liu, *Chin. J. Catal.* **37** (2016) 1413–1422.
- [6] J.S. Martinez-Espin, M. Mortén, T.V.W. Janssens, S. Svelle, P. Beato, U. Olsbye, *Catal. Sci. Technol.* **7** (2017) 2700.
- [7] L. Zhang, S. Wang, Z. Qin, P. Wang, G. Wang, M. Dong, W. Fan, J. Wang, *Molec. Catal.* **516** (2021) 111968.
- [8] N. Tsunoi, R. Osuga, M. Yasumoto, T. Yokoi, *Appl. Catal., A* **620** (2021) 118176.
- [9] S. Lin, Y. Zhi, W. Zhang, X. Yuan, C. Zhang, M. Ye, S. Xu, Y. Wei, Z. Liu, *Chin. J. Catal.* **46** (2023) 11–27.
- [10] J. Zhang, L. Xu, Y. Zhang, Z. Huang, X. Zhang, X. Zhang, Y. Yuan, L. Xu, *J. Catal.* **368** (2018) 248–260.
- [11] S. Müller, Y. Liu, F.M. Kirchberger, M. Tonigold, M. Sanchez-Sanchez, J.A. Lercher, *J. Am. Chem. Soc.* **138** (2016) 15994–16003.
- [12] X. Sun, S. Mueller, H. Shi, G.L. Haller, M. Sanchez-Sanchez, A.C. Van Veen, J. A. Lercher, *J. Catal.* **314** (2014) 21–31.
- [13] J. Valecillos, G. Elordi, A.T. Aguayo, P. Castaño, *Catal. Sci. Technol.* **11** (2021) 1269–1281.
- [14] M. Ibañez, P. Pérez-Urriarte, M. Sánchez-Contador, T. Cordero-Lanzac, A.T. Aguayo, J. Bilbao, P. Castaño, *Catalysts* **7** (2017) 254.
- [15] A.S. Al-Dughaiher, H. De Lasa, *Ind. Eng. Chem. Res.* **53** (2014) 15303–15316.
- [16] P. Pérez-Urriarte, M. Gamero, A. Ateka, M. Díaz, A.T. Aguayo, J. Bilbao, *Ind. Eng. Chem. Res.* **55** (2016) 1513–1521.
- [17] W. Dai, X. Wang, G. Wu, N. Guan, M. Hunger, L. Li, *ACS Catal.* **1** (2011) 292–299.
- [18] M. Boronat, P. Viruela, A. Corma, *Phys. Chem. Chem. Phys.* **2** (2000) 3327–3333.
- [19] W. Dai, G. Cao, L. Yang, G. Wu, M. Dybala, M. Hunger, N. Guan, L. Li, *Catal. Sci. Technol.* **7** (2017) 607–618.
- [20] D. Mores, J. Kornatowski, U. Olsbye, B.M. Weckhuysen, *Chem. -Eur. J.* **17** (2011) 2874–2884.
- [21] S. Bailleul, I. Yarulina, A.E.J. Hoffman, A. Dokania, E. Abou-Hamad, A. D. Chowdhury, G. Pieters, J. Hajek, K. De Wispelaere, M. Waroquier, J. Gascon, V. Van Speybroeck, *J. Am. Chem. Soc.* **141** (2019) 14823–14842.
- [22] C.Y. Hsieh, Y.Y. Chen, Y.C. Lin, *Ind. Eng. Chem. Res.* **57** (2018) 7742–7751.
- [23] D. Zhang, H. Liu, L. Ling, H. Zhang, R. Zhang, P. Liu, B. Wang, *Phys. Chem. Chem. Phys.* **23** (2021) 10988–11003.
- [24] T. Xia, Y. Sun, S. Han, Q. Li, *J. Phys. Chem. C.* **127** (2023) 20662–20682.
- [25] A. Wang, P. He, M. Yung, H. Zeng, H. Qian, H. Song, *Appl. Catal., B* **198** (2016) 480–492.

- [26] P. He, R. Gatip, M. Yung, H. Zeng, H. Song, *Appl. Catal.*, B 211 (2017) 275–288.
- [27] X. Shen, J. Kang, W. Niu, M. Wang, Q. Zhang, Y. Wang, *Catal. Sci. Technol.* 7 (2017) 3598–3612.
- [28] Y. Ni, W. Zhu, Z. Liu, *J. Energy Chem.* 54 (2021) 174–178.
- [29] K. Wang, M. Dong, X. Niu, J. Li, Z. Qin, W. Fan, J. Wang, *Catal. Sci. Technol.* 8 (2018) 5646–5656.
- [30] Y. Bi, Y. Wang, X. Chen, Z. Yu, L. Xu, *Chin. J. Catal.* 35 (2014) 1740.
- [31] X. Niu, J. Gao, Q. Miao, M. Dong, G. Wang, W. Fan, Z. Qin, J. Wang, *Micro Mesopor. Mat.* 197 (2014) 252–261.
- [32] Y.Z. Tzeng, C.J. Chang, M.C. Yang, M.J. Tsai, K. Teramura, T. Tanaka, H.V. Lee, J. C. Juan, J.Y. Wu, Y.C. Lin, *Catal. Today* 375 (2021) 70–78.
- [33] Z. Wei, L. Chen, Q. Cao, Z. Wen, Z. Zhou, Y. Xu, X. Zhu, *Fuel Process. Technol.* 162 (2017) 66–77.
- [34] J. Valecillos, E. Epelde, J. Albo, A.T. Aguayo, J. Bilbao, P. Castaño, *Catal. Today* 348 (2020) 243–256.
- [35] I. Pinilla-Herrero, E. Borfecchia, J. Holzinger, U.V. Mentzel, F. Joensen, K. A. Lomachenko, S. Bordiga, C. Lamberti, G. Berlier, U. Olsbye, S. Svelle, J. Skibsted, P. Beato, *J. Catal.* 362 (2018) 146–163.
- [36] H. Tian, J. Jiao, H. Tian, H. He, F. Zha, X. Guo, X. Tang, Y. Chang, *Fuel* 302 (2021), 121224–121224.
- [37] G.Q. Zhang, T. Bai, T.F. Chen, W.T. Fan, X. Zhang, *Ind. Eng. Chem. Res.* 53 (2014) 14932–14940.
- [38] Z.N. Lashchinskaya, A.A. Gabrienko, S.S. Arzumanov, A.A. Kolganov, A. V. Toktarev, D. Freude, J. Haase, A.G. Stepanov, *ACS Catal.* 10 (2020) 14224–14233.
- [39] G. Fleury, M.B.J. Roeffaers, *Catalysts* 10 (2020) 1331.
- [40] X. Su, K. Zhang, Y. Snatenkova, Z. Matieva, X. Bai, N. Kolesnichenko, W. Wu, *Fuel Process. Technol.* 198 (2020) 106242.
- [41] T. Fu, Y. Guo, J. Shao, Q. Ma, Z. Li, *Micro Mesopor. Mat.* 320 (2021) 111103.
- [42] M. Gamero, B. Valle, P. Castaño, A.T. Aguayo, J. Bilbao, *J. Ind. Eng. Chem.* 61 (2018) 427–436.
- [43] F. Liu, X. Wang, F. Xu, Q. Lin, H. Pan, H. Wu, J. Cao, *Micro Mesopor. Mat.* 252 (2017) 197–206.
- [44] Y. Xin, P. Qi, X. Duan, H. Lin, Y. Yuan, *Catal. Lett.* 143 (2013) 798–806.
- [45] S.B. Fan, D. Wang, H.B. Li, J. Tuo, X.L. Zhang, X.H. Gao, T.S. Zhao, *Appl. Catal.*, A 599 (2020) 117602.
- [46] C. Liu, E.A. Uslamin, E. Khramenkova, E. Sireci, L.T.L.J. Ouwehand, S. Ganapathy, F. Kapteijn, E.A. Pidko, *ACS Catal.* 12 (2022) 3189–3200.
- [47] I. Yarulina, A.D. Chowdhury, F. Meirer, B.M. Weckhuysen, J. Gascon, *Nat. Catal.* 1 (2018) 398–411.
- [48] I. Yarulina, S. Bailleul, A. Pustovarenko, J.R. Martinez, K.D. Wispelaere, J. Hajek, B.M. Weckhuysen, K. Houben, M. Baldus, V. Van Speybroeck, F. Kapteijn, J. Gascon, *ChemCatChem* 8 (2016) 3057–3063.
- [49] A. Liutkova, H. Zhang, J.F.M. Simons, B. Mezari, M. Mirolo, G.A. Garcia, E.J. M. Hensen, N. Kosinov, *ACS Catal.* (2023) 3471–3484.
- [50] C.A. Emeis, *J. Catal.* 141 (1993) 347–354.
- [51] M. Ghaedi, A. Izadbakhsh, *J. Fuel Chem. Technol.* 49 (2021) 1468–1486.
- [52] H. Khezri, A. Izadbakhsh, A.A. Izadpanah, *Fuel Process. Technol.* 199 (2020) 106253.
- [53] Y. Yuan, R.F. Lobo, *ACS Catal.* 13 (2023) 4971–4984.
- [54] L.H. Ong, M. Dömök, R. Olindo, A.C. van Veen, J.A. Lercher, *Micro Mesopor. Mat.* 164 (2012) 9–20.
- [55] M. Ibáñez, M. Artetxe, G. Lopez, G. Elordi, J. Bilbao, M. Olazar, P. Castaño, *Appl. Catal.*, B 148–149 (2014) 436–445.
- [56] A.A. Gabrienko, I.G. Danilova, S.S. Arzumanov, L.V. Pirutko, D. Freude, A. G. Stepanov, *J. Phys. Chem. C.* 122 (2018) 25386–25395.
- [57] J. Li, T. Li, H. Ma, Q. Sun, W. Ying, D. Fang, *Ind. Eng. Chem. Res.* 54 (2015) 1796–1805.
- [58] J.-W. Li, T. Li, H.-F. Ma, Q.-W. Sun, W.-Y. Ying, D.-Y. Fang, *Fuel Process. Technol.* 159 (2017) 31–37.
- [59] R. Jin, K. Ma, Z. Chen, Z. Tang, H. Hu, J. Wang, Z. Zhang, C. Dai, X. Ma, *Fuel* 332 (2023) 126247.
- [60] X. Liu, C. Yan, Y. Wang, P. Zhang, S. Yan, H. Wang, J. Zhuang, Y. Zhao, Y. Wang, Y. Yu, Q. Zhao, X. Zhu, F. Yang, *Chem. Eng. Sci.* 270 (2023) 118542.
- [61] S.M.T. Almutairi, B. Mezari, P.C.M.M. Magusin, E.A. Pidko, E.J.M. Hensen, *ACS Catal.* 2 (2012) 71–83.
- [62] M. Avramovska, D. Freude, J. Haase, A.V. Toktarev, S.S. Arzumanov, A. A. Gabrienko, A.G. Stepanov, *Phys. Chem. Chem. Phys.* 25 (2023) 28043–28051.
- [63] M. Bjørgen, S. Svelle, F. Joensen, J. Nerlov, S. Kolboe, F. Bonino, L. Palumbo, S. Bordiga, U. Olsbye, *J. Catal.* 249 (2007) 195–207.
- [64] J. Valecillos, I. Hita, E. Sastre, A.T. Aguayo, P. Castaño, *ChemCatChem* 13 (2021) 3140–3154.
- [65] N. García-Gómez, J. Valecillos, A. Remiro, B. Valle, J. Bilbao, A.G. Gayubo, *Appl. Catal.*, B 297 (2021) 120445.
- [66] L. Landa, A. Remiro, J. Valecillos, B. Valle, J. Bilbao, A.G. Gayubo, *Fuel* 321 (2022) 124009.
- [67] N. Nesterenko, J. Aguilhon, P. Bodart, D. Minoux, J.P. Dath, in: B.F. Sels, L. M. Kustov (Eds.), Chapter 5 - Methanol to Olefins: An Insight Into Reaction Pathways and Products Formation: Zeolites and Zeolite-like Materials, Elsevier Inc, The Netherlands, 2016, pp. 189–263.
- [68] A.G. Gayubo, A.T. Aguayo, A. Atutxa, R. Prieto, J. Bilbao, *Ind. Eng. Chem. Res.* 43 (2004) 5042–5048.
- [69] A. Liutkova, N. Kosinov, E.J.M. Hensen, *J. Catal.* 428 (2023) 115169.
- [70] M. DeLuca, D. Hibbitts, *Micro Mesopor. Mat.* 333 (2022) 111705.
- [71] M. Luo, Y. Fu, B. Hu, D. Wang, B. Wang, G. Mao, *Appl. Catal.*, A 570 (2019) 209–217.
- [72] Y. lun Wang, H. hui An, H. Ma, X. chun Zhang, G. jun Kang, J. pei Cao, *Adv. Powder Technol.* 32 (2021) 1869–1880.
- [73] L. Yang, Z. Liu, Z. Liu, W. Peng, Y. Liu, C. Liu, *Chin. J. Catal.* 38 (2017) 683–690.
- [74] W. Dai, N. Li, L. Li, N. Guan, M. Hunger, *Catal. Commun.* 16 (2011) 124–127.
- [75] Y. Ji, H. Yang, W. Yan, *Catalysts* 7 (2017) 367.
- [76] Z. Chen, Y. Hou, W. Song, D. Cai, Y. Yang, Y. Cui, W. Qian, *Chem. Eng. J.* 371 (2019) 639–646.